

FAST REMOVAL OF METHYLENE BLUE FROM AQUEOUS SOLUTION BY ADSORPTION ONTO POORLY CRYSTALLINE HYDROXYAPATITE NANOPARTICLES

W. WEI^{a,b}, L. YANG^a, W.H. ZHONG^a, S.Y. Li^a, J. CUI^a, Z.G. WEI^{a,b*}

^a*Jiangsu Provincial Key Laboratory of Materials Cycling and Pollution Control, Department of Environmental Science and Engineering, Nanjing Normal University, Nanjing 210023, China*

^b*Jiangsu Center for Collaborative Innovation in Geographical Information Resource Development and Application, Nanjing 210023, China*

A novel poorly crystalline hydroxyapatite (HAP) nanomaterial was developed for methylene blue (MB) removal from aqueous solution. Surface functionality, crystallinity, and morphology of the synthetic adsorbent were characterized and the potential of poorly crystalline HAP nanoparticles for MB removal was evaluated. Results indicated that poorly crystalline HAP nanoparticles possessed good adsorption ability to MB. The adsorption process was fast, and it reached a steady state after only 2 min. MB removal was increased with an increasing amount of adsorbent dosage but decreased as the ionic strength increased. It was worth noting that the presence of humic acid significantly promoted the adsorption of MB by poorly crystalline HAP. While the adsorption was favorable at higher pH and lower temperature, and the equilibrium data were well fitted by the Freundlich isotherm. The maximum adsorption capacity was estimated to be 14.27 mg/g. Thermodynamic parameters suggested that the adsorption was a typical physical process, spontaneous, and exothermic in nature. The mechanisms for the adsorption of MB on poorly crystalline HAP may include electrostatic attraction, hydrogen bonding, and Lewis acid-base interaction. Regeneration studies exhibited that HAP could be recyclable for a long term. The obtained results indicated that poorly crystalline HAP nanoparticles can be used as a biocompatible and effective adsorbent to remove MB from water.

(Received September 30, 2015; Accepted November 25, 2015)

Keywords: Hydroxyapatite, crystallinity, Biocompatible adsorbent, Isotherm, Methylene blue

1. Introduction

Dyes are important raw materials of textile, dyeing, printing and other related industries. Discharge of wastewater containing dye compounds into water sources will deplete the dissolved oxygen content in water and also inhibit sunlight from reaching to the water sources [1]. Since many organic dyes are harmful to human being and toxic to microorganisms, removal of dyes from wastewater has long been a major environmental problem all over the world. As one of the common dyes, methylene blue (MB) is widely used as the coloring agent and disinfectant in rubbers, pharmaceuticals, pesticides, varnishes, and dyestuffs and so on [2]. It has been reported that cationic dyes like MB are more toxic than anionic dyes [3]; although MB is not strongly hazardous, exposure of MB and/or other dyes to human being will cause skin and eye irritation,

*Corresponding author: weizhenggui@gmail.com

carcinogenicity, reproductive and developmental toxicity, neurotoxicity and chronic toxicity [4,5]. Therefore, an increased interest has been focused on removing of MB and other dyes from the wastewater.

Various methods have been developed for dyes removal including biological treatment [6], coagulation [7], chemical oxidation and photocatalytic processes [8,9], membrane separation [10], electrochemical process [11], and adsorption techniques [12-15]. However, due to the complex aromatic molecular structures, dyes are resistant to light, temperature, degradation and many chemicals, and cannot be completely removed by conventional methods [16]. As a result, many biological and/or chemical treatment processes are usually restricted due to little applicability to a wide range of wastewater and high operating cost. By contrast, the adsorption process is arguably one of the most popular methods for dyes removal and has attracted considerable attention because of its simplicity of design, ease of operation and high efficiency.

At present, the search for low-cost and easily available adsorbents has led many researchers to explore more economic and efficient techniques of using the natural and synthetic materials as adsorbents [17-21]. Among them, nanomaterial represents a promising application in a variety of fields due to the special properties [22]. One of its properties is that most of the atoms of the nanoparticle are on the surface. The surface atoms are unsaturated and can therefore bind with other atoms, possess highly chemical activity and adsorption ability [23]. In this view, nanomaterial is the most promising candidate for dyes removal from aqueous solution. For instance, barium phosphate nano-flake [2], chitosan/Fe-hydroxyapatite nanocomposite [18], acid-bound iron oxide magnetic nanoparticles [24], humic-acid coated magnetic nanoparticles [25], carboxymethyl- β -cyclodextrin conjugated magnetic nano-adsorbent [26], humic acid-coated Fe₃O₄ nanoparticles [27], halloysite nanotubes [28], alkali-activated multiwalled carbon nanotubes [29], Co₃O₄/SiO₂ nanocomposite [30], and magnetite loaded multi-wall carbon nanotube [31] etc., have been used to eliminate aqueous MB because of their strong affinity for MB. However, most of these composite nano-adsorbents suffer from high cost and/or the utilization of some environmentally incompatible additives. Therefore, the development of cheaper, more effective and biocompatible nanomaterial-based adsorbent is needed for MB removal.

Currently, the application of apatite materials for the adsorption and immobilization of various pollutants has been considered as a promising pollution control technology, due to the low cost, high efficiency, easy-to-implement, and environmental friendly nature [32]. Apatite is a general name for different minerals with the formula X₁₀(YO₄)₆(OH, F, Cl)₂, where X can be any of several metal cations such as calcium, barium, sodium, lead, strontium, etc., and Y can be phosphorous, vanadium or arsenic [33]. Generally, hydroxyapatite [Ca₁₀(PO₄)₆(OH)₂, HAP] is most commonly found in nature as a member of the apatite mineral group and also can be produced through precipitation from calcium phosphate solutions. In addition, HAP is a major mineral component of bones and teeth of vertebrates. The structure of HAP is hexagonal, with space group P6₃/m: essentially a 6-fold *c*-axis perpendicular to three equivalent *a*-axes at angles of 120° to each other [34]. Due to its special chemical composition and crystal structure, together with the excellent biocompatibility and adsorption properties, HAP has been widely used as an environmental benign functional material for adsorption of heavy metals [32], fluoride [35,36], phenol [37], fulvic acid [38], arsenic [39], and dyes [40-42] from contaminated soil and water. However, although there are several reports on adsorption of dyes such as disperse blue SBL [40], reactive yellow 4 [41], direct yellow 27 [42], and reactive blue 204 [17] onto HAP, no work has

been done to our knowledge, on adsorption of MB by HAP nanoparticles.

Moreover, crystallinity of HAP adsorbent is believed to be an important factor affecting the adsorption capacity for adsorbate; inducing low crystallinity of adsorbent will significantly enhance the surface area and reduce the particle size, accompanied by a concomitant rise in the quantity of active sites on adsorbent surface, which will cause a remarkable enhancement of the adsorption ability. Higher adsorption capacities for fluoride and fulvic acid of the poorly crystalline HAP have been reported in our previous work [35,38]. However, little knowledge is available about the adsorption behaviors and influencing factors of MB onto HAP nanoparticles, and information concerning the interaction mechanisms of MB with poorly crystalline HAP nanoparticles is even more deficient.

The aim of this study was to evaluate the ability of using poorly crystalline HAP nanoparticles prepared by an improved neutralization method for the adsorption of MB from aqueous solution. The effects of contact time, adsorbent dosage, temperature, pH, ionic strength, and the presence of humic acid on MB adsorption were investigated in detail. The Langmuir, Freundlich and Dubinin-Radushkevich (D-R) adsorption models were applied to describe the equilibrium isotherms and the isotherm constants were also determined. The possible mechanisms for MB adsorption onto poorly crystalline HAP nanoparticles were proposed.

2. Materials and methods

2.1 Materials

For the preparation of HAP nanoparticles, CaCO_3 and H_3PO_4 were purchased from Sinopharm Chemical Reagent Company (Shanghai, China). MB, $\text{C}_{16}\text{H}_{18}\text{ClN}_3\text{S}\cdot 3\text{H}_2\text{O}$ supplied by Sigma-Aldrich was used as adsorbate and was not purified prior to use. The molecular structure of MB is shown in Figure 1. All chemicals used in this study were of commercially available analytical grade and used as received without further purification. Milli-Q water was used throughout this study.

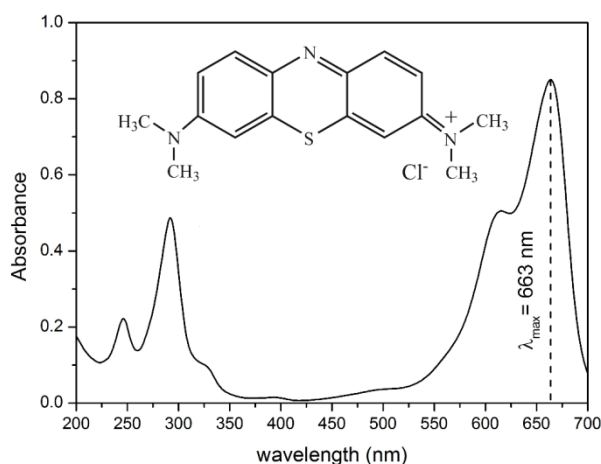


Fig. 1. Molecular formula and UV-visible spectrum of Methylene blue.

2.2 Preparation and characterization of adsorbent

In this study, HAP nanoparticles were prepared by a novel neutralization method with the assistance of ultrasonic irradiation. This method was described in detail in our previous work [43]. Briefly, the $\text{Ca}(\text{OH})_2$ suspension was prepared by slurring CaO powder (obtained by calcination of CaCO_3 at $1100\text{ }^\circ\text{C}$ for 24 h) into freshly double distilled water. The suspension was then exposed to an ultrasonic irradiation source of 50 W at maximum amplitude for 1 h. Then a required amount of H_3PO_4 was added dropwise to $\text{Ca}(\text{OH})_2$ suspension while undergoing a second hour of ultrasonic irradiation. During the synthesis process the Ca:P ratio was kept at 1.667. Intensive stirring and slow reagent addition were applied for the purpose of avoiding a local inhomogeneity. After complete addition, the resultant white slurry ($\text{pH} = 7.0$) was centrifuged at $10,000 \times g$ for 30 min. Then the precipitated HAP was washed with double distilled water and separated from the suspension by vacuum filtration. The resultant powders were dried at $80\text{ }^\circ\text{C}$ for 24 h, and then calcined at $100\text{ }^\circ\text{C}$ for 1 h to obtain poorly crystalline HAP nanoparticles.

The phase purity and crystallinity of the prepared HAP were determined by powder XRD using $\text{Cu K}\alpha$ ($\lambda=1.5405\text{ \AA}$) radiation on a Rigaku D/max-III B X-ray powder diffractometer. The morphology and size of the prepared HAP were characterized by a Hitachi Model H-7650 transmission electron microscope. The TEM sample was prepared by depositing a few drops of the HAP particles ultrasonically dispersed in ethanol for 30 min on a carbon-coated copper grid. The specific surface area of synthetic HAP was determined by nitrogen adsorption at 77 K (Micromeritics ASAP 2010). Surface area was calculated from adsorption data using BET equation. And batch equilibration technique was applied to determine pH_{PZC} (point of zero charge) of prepared HAP [44]. The FTIR spectra of HAP before and after the adsorption of HA were recorded on a Thermo Scientific Nicolet iS5 FTIR spectrometer with the KBr pellet technique.

2.3 Batch adsorption experiments

The batch adsorption test was carried out by shaking 100 mL of MB solution with 20-200 mg of adsorbent in stoppered conical flasks. The flasks were shaken on a shaker equipped with thermostat at 200 rpm and at specified temperature. After a predetermined contact time, the flasks were removed from the shaker and the supernatant was centrifuged at 6000 rpm for 15 min and analyzed for MB concentration. The effects of contact time, dye concentration, pH, temperature and adsorbent dosage on adsorption were evaluated by batch adsorption experiments. To determine the calibration curve of MB, absorbance of solutions with predetermined MB concentrations at $\lambda_{\text{max}} = 663\text{ nm}$ was detected by UV-Vis spectrophotometer (UV-2450, Shimadzu). In the following adsorption experiments, the concentration of the MB solution after absorption will be determined by using this calibration curve, and the equilibrium adsorption capacity, q_e (mg/g) and removal rate (%), are expressed as follows: $q_e = (C_0 - C_e)V/m$ and removal rate (%) = $(C_0 - C_e)/C_0$, where C_0 and C_e are the initial and equilibrium concentrations of MB (mg/L) in solution; V (L) is the volume of aqueous solution containing MB; and m (g) is the weight of adsorbent. All adsorption experiments were conducted in triplicates and the results were reported as average.

2.4 Desorption and reuse study

Regeneration and reuse of adsorbent is of great importance in practical applications. Desorption results can also be used to investigate the mechanism of the adsorption and desorption processes. For desorption experiment, the MB-adsorbed poorly crystalline HAP was washed

thoroughly with deionized water. Desorption of MB was then performed by putting the MB-adsorbed nanoparticles into phosphate solution. After mixing for several minutes and removing the nanoparticles, the concentration of MB in liquid solution was measured to estimate the amount of MB desorbed.

3. Results and discussion

3.1 Characterization of the prepared HAP

Fig. 2a showed the XRD pattern of the prepared HAP sample. The synthetic sample was in good agreement with the reference pattern of pure HAP (JCPDS no. 09-0432), and no characteristic peaks of impurities, such as calcium hydroxide and calcium phosphates, were observed, meaning that phase pure HAP were obtained under the present experimental conditions. Moreover, according to the XRD spectra, the characteristic peaks of HAP sample were very broad, indicating that it was composed of small-sized and poorly crystalline HAP. From XRD data, the fraction of the crystalline phase (X_c) in HAP sample could be determined as: $X_c = 1 - (V_{112/300}/I_{300})$, where $V_{112/300}$ represented the intensity of the hollow between diffraction peaks (112) and (300), and I_{300} was the intensity of (300) diffraction peak [45]. The average particle size (D) of the synthetic HAP samples could be calculated from the XRD line broadening measurement from the Scherrer formula [46]: $D = 0.89\lambda/\beta\cos\theta$, where λ is the X-ray wavelength (1.5405 Å), β is the full width at the half maximum of the HAP (211) line and θ is the diffraction angle. The crystallinity and average particle size of the synthetic HAP were found to be 0.28 and 35 nm, respectively.

The typical TEM image of the HAP sample was shown in Figure 2b. It indicated that the HAP particles were needle-like nanocrystals with almost no amorphous constituents and weakly aggregated. The particle size estimated from TEM micrographs was less than 40 nm, which was consistent with the XRD data. FT-IR spectra of HAP before and after adsorption were shown in Figure 3. The FT-IR spectrum of HAP showed the characteristic bands for PO_4^{3-} (566, 603, 962, 1043 and 1092 cm^{-1}), and the phosphate bond stretching occurring at 962 cm^{-1} indicated the crystalline structure of the apatite phase formation [35]. While a weak sharp peak at 3568 cm^{-1} corresponded to the stretching vibration of the lattice OH^- ions, and a peak at 630 cm^{-1} was assigned to the O-H bending deformation mode, indicating the formation of pure HAP [36]. The broad bands at 1632 and 3447 cm^{-1} were attributed to adsorbed water, while some carbonate derived bands were observed around 1420 and 1458 cm^{-1} . It might be due to the adsorption of atmospheric carbon dioxide during the sample preparation. This small amount of carbonate has not produced either carbonate substituted HAP (as evident by XRD) or other carbonates [43]. After the MB adsorption, most of these characteristic peaks of MB-loaded HAP remained the same as those of HAP, suggesting that the process of MB adsorption on the HAP was mainly a physical adsorption.

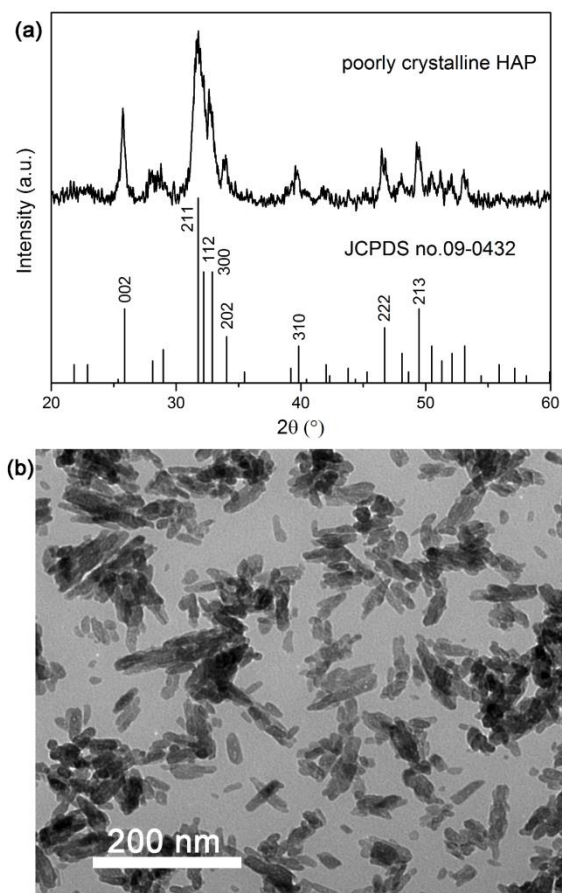


Fig. 2. (a) The XRD patterns of the synthetic HAP and the reference pattern of pure HAP (JCPDS no. 09-0432). (b) The TEM micrograph of the synthetic HAP

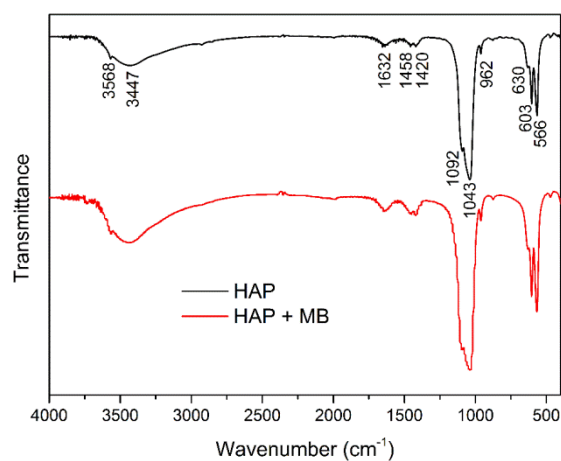


Fig. 3. FTIR spectra of poorly crystalline HAP before (a) and after (b) adsorption of the MB

The surface area of HAP nanoparticles measured by the BET method was determined to be $73.6 \text{ m}^2/\text{g}$. The pH_{PZC} is a concept related to the phenomenon of adsorption that describes the condition when the electrical charge density on the adsorbent surface is zero. The pH_{PZC} was found to be 6.3 for the synthetic poorly crystalline HAP sample.

3.2 Effects of contact time and adsorbent dosage on MB adsorption

Fig. 4a showed the effect of contact time on adsorption of MB onto poorly crystalline HAP nanoparticles under various initial concentrations of MB and at 25 °C.

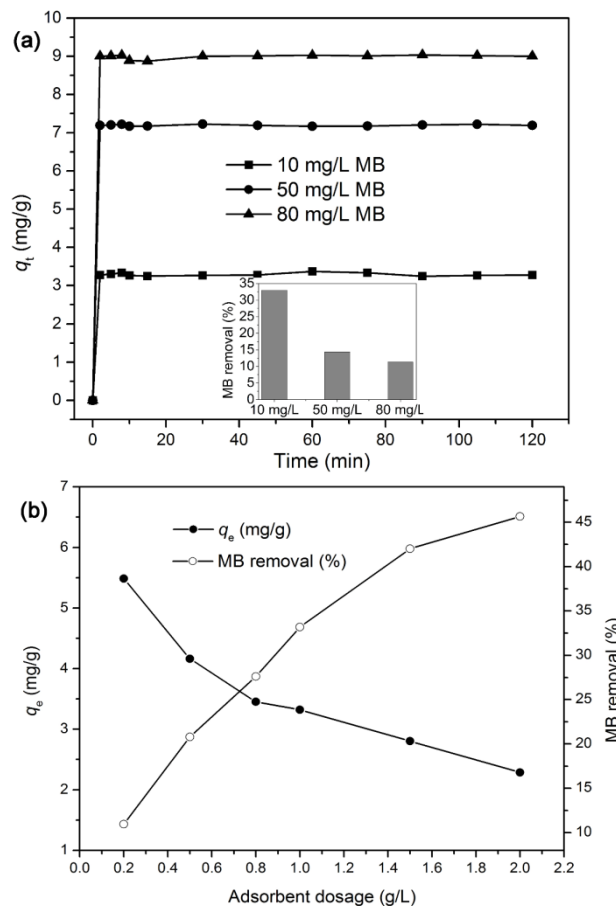


Fig. 4. Effect of contact time (a) and adsorbent dosage (b) on MB adsorption by poorly crystalline HAP (adsorption conditions: adsorbent dosage = 1 g/L, initial pH 9.0, and temperature = 298 K).

The initial MB concentration provided the necessary driving force to overcome the mass transfer resistance of MB between the aqueous and solid phases [26]. It was obvious that the adsorption equilibrium of MB was obtained within 1 min for the initial MB concentration of 10, 50, and 80 mg/L, respectively. Thereafter, no detectable concentration changes occurred after adsorption equilibrium (2 min) and the average removal efficiency of MB reached about 33.0% (3.30 mg/g adsorption capacity), 14.4% (7.21 mg/g adsorption capacity), and 11.3% (9.03 mg/g adsorption capacity) when the initial concentrations of MB were 10, 50, and 80 mg/L, respectively. The short equilibrium time indicated high adsorptive reaction rate of poorly crystalline HAP, which was significant in practical applications. Such a fast adsorption rate could be attributed to the absence of internal diffusion resistance [26], and this suggested that poorly crystalline HAP could rapidly and effectively adsorb MB from aqueous solution. The equilibrium time of different initial MB concentrations was also conducted and the results showed that the initial MB concentrations had little effect on the adsorption equilibrium time. Additionally, Figure 4a also illustrated that MB removal rate decreased with increase in initial MB concentration, but the actual

amount of MB adsorbed per unit mass of HAP increased with increase in MB concentration. The reason was the limited number of adsorption sites available for the uptake of MB at a fixed adsorbent dosage.

The effect of adsorbent dosage was studied with different adsorbent dosages (0.2-2.0 g/L) and 100 mL of 10 mg/L MB solutions at pH 9.0. As shown in Figure 4b, increase in adsorbent dosage increased the removal rate for MB. With the increase in HAP dosage from 0.2 to 2.0 g/L, the MB removal efficiency increased rapidly from 11.0 to 45.7%. The reason for such behavior might be attributed to greater surface area and large number of vacant adsorption sites thus favoring more MB adsorption. The results also demonstrated that it was possible to remove MB completely when there was sufficient poorly crystalline HAP surface area in solution. In this study, the optimized adsorbent dosage was fixed at 1.0 g/L for further experiments. On the other hand, adsorption capacity of MB was decreased with an increase in adsorbent dosage. As the adsorbent dose was increased from 0.2 to 2.0 g/L, the adsorption capacity for MB decreased from 5.49 to 2.28 mg/g. The decrease in adsorption capacity with the increase in the adsorbent dosage has been extensively reported in literature [14,16], which was mainly attributed to the unsaturation of adsorption sites during the adsorption process.

3.3 Effect of pH on MB adsorption

The pH of the dye solution is an important factor controlling adsorption processes, particularly the adsorption capacity. The efficiency of adsorption is dependent on the solution pH because variation in pH leads to the variation in the degree of ionization of the adsorptive molecule and the surface properties of adsorbent [13]. The adsorption of MB onto poorly crystalline HAP was studied at different initial pH between 3.0 and 10.0. Figure. 5a showed that an increase in solution pH from 3 to 10 caused an obvious increase in the MB adsorption capacity for poorly crystalline HAP from 2.798 to 4.390 mg/g (10 mg/L MB). It could be seen that the MB adsorption was highly pH-dependent and the adsorption of MB on poorly crystalline HAP was favored at higher pH value.

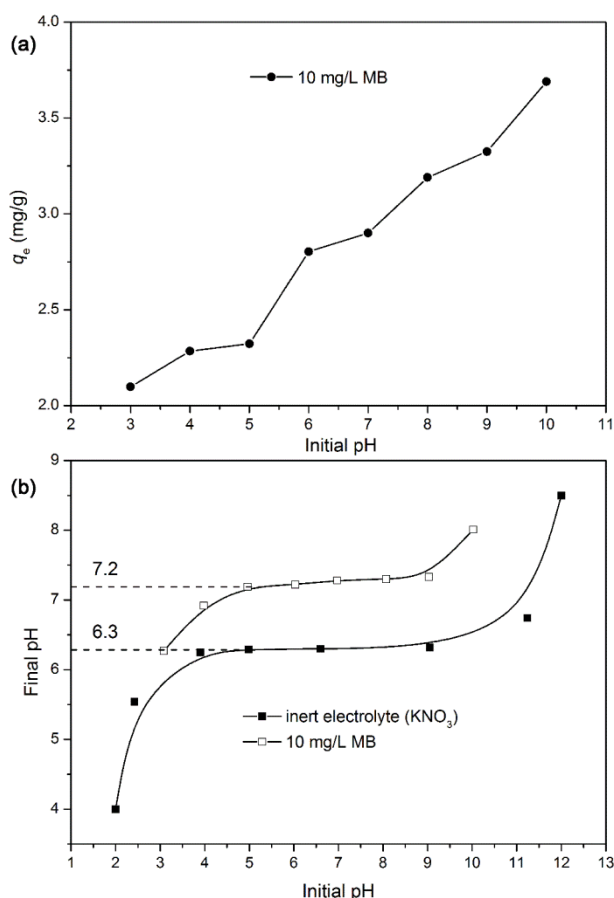
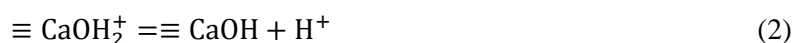


Fig. 5. (a) Effect of pH on the adsorption of MB onto poorly crystalline HAP; (b) Relationships between initial pH, final pH values obtained after equilibration of HAP with MB solution and inert electrolyte. (adsorption conditions: adsorbent dosage = 1.0 g/L, temperature = 298 K)

It has been reported that MB was a very weak base and reacted only in the solutions of strong acids to yield low amounts of protonated cations; therefore, it was considered that MB is a positively charged, unprotonated cation, throughout the pH range investigated [47]. In the case of poorly crystalline HAP, it was generally accepted that HAP exhibited amphoteric properties, and acted as a buffer in a rather large pH range [48]; the buffering characteristics and surface charge of HAP were expected to be the result of acid-base interactions of the reactive surface sites. According to Wu et al. [49], the reactions responsible for the surface properties of HAP in aqueous solutions are:



The pH_{PZC} of the poorly crystalline HAP was determined to be 6.3 and the variation in final pH after interaction of HAP with MB solution, were also plotted as a function of the initial pH (Figure 5b). In the low pH conditions (below pH_{PZC}), the consumption of protons from the solution by the protonation of negatively charged ($\equiv \text{PO}^-$) and neutral ($\equiv \text{CaOH}$) surface groups

resulted in final pH increase (Figure 5b), while the positively charged $\equiv\text{CaOH}_2^+$ and neutral $\equiv\text{P-OH}$ sites prevail on HAP surface, making surface charge of HAP positive in this pH region. In this case, positively charged surface sites on HAP did not favor the adsorption of dye cations due to the electrostatic repulsion. Furthermore, lower adsorption of MB at acidic pH might also be explained by the competition of excess H^+ with the dye cation for active adsorption sites. However, despite the electrostatic repulsion and/or H^+ competition a considerable amount of MB was adsorbed by poorly crystalline HAP at lower pH values (Figure 5a), which suggested that other mechanisms might involve in the MB adsorption process. It was considered that the $\equiv\text{P-OH}$ group could bind with the $=\text{N}$ of the MB molecule through hydrogen bonding which also contributed toward adsorption of MB molecules onto poorly crystalline HAP nanoparticles [50]. In addition, the nitrogen atom of MB might interact with Ca^{2+} groups of HAP via Lewis acid-base interaction, because the MB behaved as a Lewis base, donating electron density, via the nitrogen lone pair of electrons, into the lowest lying unoccupied molecular orbitals of calcium on HAP surface [51].

On the other hand, final pH decrease (Figure 5b) took place in the range of higher initial pH (above pH_{PZC}) due to the consumption of OH^- via the deprotonation of the surface deprotonation of surface $\equiv\text{CaOH}_2^+$ and $\equiv\text{POH}$ sites and thus, neutral $\equiv\text{CaOH}$ and negatively charged $\equiv\text{PO}^-$ species predominated, causing HAP surface to become negatively charged in this pH region [49]. In addition, the pH of the final MB dye solution was the result of electrostatic interaction between negatively charged HAP adsorbent surface and cationic MB solution to form complex, and more H^+ came into solution which gave a little decrease of the final solution pH [13]. In this case, the adsorption of MB on HAP was mainly attributed to the electrostatic attraction between the positively charged MB molecules and the negatively charged HAP surface. While at pH above the pH_{PZC} of HAP, the MB molecules in solution might also interact with HAP via Lewis acid-base interaction. The possible modes of interaction of MB with the HAP surface have been gathered in Figure 6.

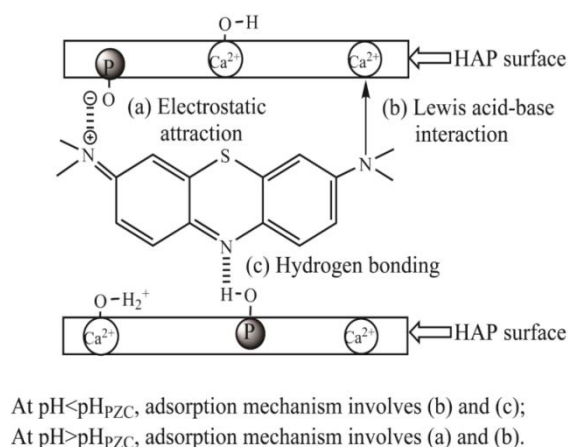


Fig. 6. Possible mechanisms for MB adsorption onto poorly crystalline HAP surface.

The monotonous increasing trend of dyes adsorption-pH relationship has been reported intensely and similar results of pH effect were also reported for the adsorption of MB on acid-bound iron oxide magnetic nanoparticles [24], humic acid-coated magnetic nanoparticles

[25,27], and jute fiber carbon [52] etc. Furthermore, it was worth noting that pH_{PZC} of HAP was shifted to the higher value in the presence of MB as illustrated in Figure 5b. The plateau part of the pH_{final} vs. $pH_{initial}$ plot, corresponding to the pH range where the buffering effect of HAP surface took place, while pH_{PZC} of HAP increased from 6.3 to 7.2. Similar findings have been reported by Senthilkumar et al. [52], who suggested that the specific cationic dyes adsorption shifted the pH_{PZC} to higher values.

3.4 Effects of ionic strength and humic acid on MB adsorption

The wastewater containing dye has commonly higher salt concentration, and effect of ionic strength are of great importance in the study of dye adsorption onto adsorbents [4]. In order to investigate the effect of inorganic salts in dye adsorption process, the experiments were carried out using 10 mg/L initial MB solution containing various NaCl or CaCl₂ concentrations ranging from 0.01 to 0.1 mol/L. In addition, humic acid (HA) is ubiquitous in natural waters and has been found to interact with nanomaterials and various pollutants including dyes. In this work, the presence of HA on the adsorption of MB by poorly crystalline HAP nanoparticles was also conducted.

As shown in Figure 7, NaCl or CaCl₂ existing in solution affected the MB adsorption onto poorly crystalline HAP. It was indicated that the adsorption capacities decreased with increasing NaCl or CaCl₂ concentration, which could be attributed to the competitive effect between MB ions and cations from the salt for the sites available for the adsorption process. As ionic strength increased from 0 to 0.1 mol/L, the amount of MB adsorbed onto HAP decreased from 3.31 to 2.78 and 2.31 mg/g for NaCl and CaCl₂, respectively, while the removal rate decreased from 33.1 to 27.8 and 23.1% for NaCl and CaCl₂. Similar findings have been reported by Han et al. [53], who pointed out that the decreasing adsorption capacities of MB could also be attributed to the activity of MB and the active sites decreased as the increasing of ionic strength. Moreover, as Ca²⁺ has more contribution to ionic strength and more positive charge than Na⁺, the effect of Ca²⁺ on adsorption is more serious than Na⁺.

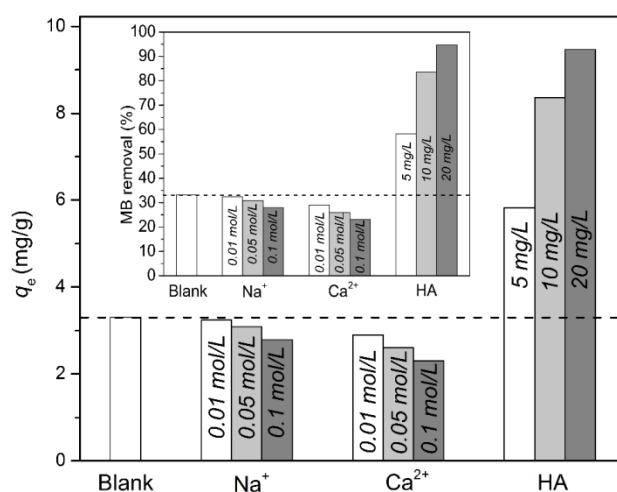


Fig. 7. Effects of ionic strength and humic acid on the adsorption of MB by poorly crystalline HAP (adsorption conditions: adsorbent dosage = 1.0 g/L, initial pH 9.0, and temperature = 298 K)

It was worth noting that the presence of HA significantly promoted the adsorption of MB by poorly crystalline HAP nanoparticles (Figure 7). As HA concentration increased from 0 to 20 mg/L, the amount of MB adsorbed onto HAP increased from 3.31 to 9.47 mg/g, while the removal rate increased from 33.1 to 94.7%. It is generally accepted that HA is a class of natural organic polymers which originates from the decomposition of plants and animal residues. HA exhibits excellent reaction activity for bearing abundant functional groups such as carboxyl, phenolic, carbonyl, and amino groups, which can bind cationic MB from aqueous solution [25]. On the other hand, since the pK_a values of carboxyl and phenolic groups were around 3.0 and 9.0, HA was expected to be negatively charged by deprotonation of carboxylic groups at pH above 3.0. And the high affinity of HA onto HAP surface has been reported in our previous work [38,43], therefore, the electrostatic attraction of cationic MB with HAP could be significantly enhanced in the presence of HA, which led to the efficient adsorption of MB onto poorly crystalline HAP nanoparticles.

3.5 Adsorption isotherms

Adsorption isotherm is the relationship between the amount of a substance adsorbed and its concentration in the equilibrium solution at constant temperature. The adsorption isotherm is important from both a theoretical and a practical point of view, because the application of adsorption isotherms facilitates describing the interaction between the adsorbate and the adsorbent of any system. The parameters obtained from the different models provide important information on the adsorption mechanisms and the surface properties and affinities of the adsorbent [54]. There are several equations for analyzing experimental adsorption equilibrium data. In the present investigation, Langmuir, Freundlich, and Dubinin-Radushkevich (D-R) isotherm models were used to describe the adsorption of HA on the poorly crystalline HAP nanoparticles:

The Langmuir isotherm assumes monolayer coverage of adsorbate on homogeneous sites of the adsorbent, uniform energy of adsorption, and no interaction between molecules adsorbed on neighboring sites. The Langmuir equation is given in the following equation [55]:

$$q_e = \frac{q_m K_L C_e}{1 + K_L C_e} \quad (3)$$

where q_e (mg/g) is the adsorption capacity at equilibrium; C_e (mg/L) is the equilibrium concentration of MB in solution; q_m (mg/g) is the maximum monolayer adsorption capacity, and K_L (L/mg) is the Langmuir equilibrium constant.

Unlike the Langmuir, Freundlich isotherm is based on adsorption to heterogeneous surface or surfaces supporting sites of varied affinities, and it is assumed that the stronger binding sites are occupied first and that the binding strength decreases with increasing degree of site occupation. The Freundlich isotherm is described by the following equation [56]:

$$q_e = K_F C_e^{1/n} \quad (4)$$

where q_e (mg/g) is the equilibrium MB concentration on the adsorbent, K_F [$\text{mg/g}(\text{L/mg})^{1/n}$] is the empirical constant of Freundlich isotherm and C_e (mg/L) is the equilibrium concentration of the MB in solution. The constant n is the empirical parameter related to the favorability of the adsorption process. When $1/n$ values are below 1, it is considered as an indication of favorable

adsorption.

The D-R isotherm equation, which is more generally applied to distinguish between physical and chemical adsorption, is represented by the following equation [57]:

$$q_e = X_m \exp(-B\varepsilon^2) \quad (5)$$

where q_e is the amount of MB adsorbed (mg/g), X_m is the maximum adsorption capacity of MB (mg/g), B is the D-R constant (mol^2/kJ^2), and ε is the Polanyi potential given by the following equation:

$$\varepsilon = RT \ln\left(1 + \frac{1}{C_e}\right) \quad (6)$$

where R is the gas constant in J/mol K, T is the temperature (K) and C_e is the equilibrium concentration of Cu(II) (mg/L). The constant B is related to the mean free energy (E) of adsorption and this can be computed using the following relationship:

$$E = \frac{1}{\sqrt{2B}} \quad (7)$$

Figs. 8(a-c) showed the nonlinear plot for MB adsorption onto poorly crystalline HAP based on nonlinear Langmuir, Freundlich and D-R isotherm models. The obtained values for Langmuir, Freundlich and D-R isotherm constants and correlation coefficients were listed in Table 1. The obtained correlation coefficient (R^2) of Freundlich was higher than that of Langmuir and D-R models, suggesting that the adsorption data were well described by Freundlich isotherm model and supported the assumption that MB was heterogeneously adsorbed onto the surface of poorly crystalline HAP. It was generally considered that HAP surface was heterogeneous with "C" and "P" sites [43], which were responsible for the heterogeneous adsorption of MB onto HAP. Value of $1/n$ in Freundlich model was considered as an indication of how favorable the adsorption process. When the values of $1/n$ were in the range of 0.1-1, the adsorption process was favorable. The values of $1/n$ were between 0.4648 and 0.3994 for different temperatures, indicating a high affinity of HAP for MB and the great heterogeneity of HAP surface. Generally, K_F was roughly an indicator of the adsorption capacity. From the non-linear plots of the Freundlich isotherm, the values of K_F were 1.36, 1.26 and 1.13 [$\text{mg/g}(\text{L}/\text{mg})^{1/n}$] at 283, 298 and 313 K, respectively. The values of K_F increased with the decrease in the temperatures, indicating that the adsorption capacity of MB on HAP increased with the decrease of temperatures.

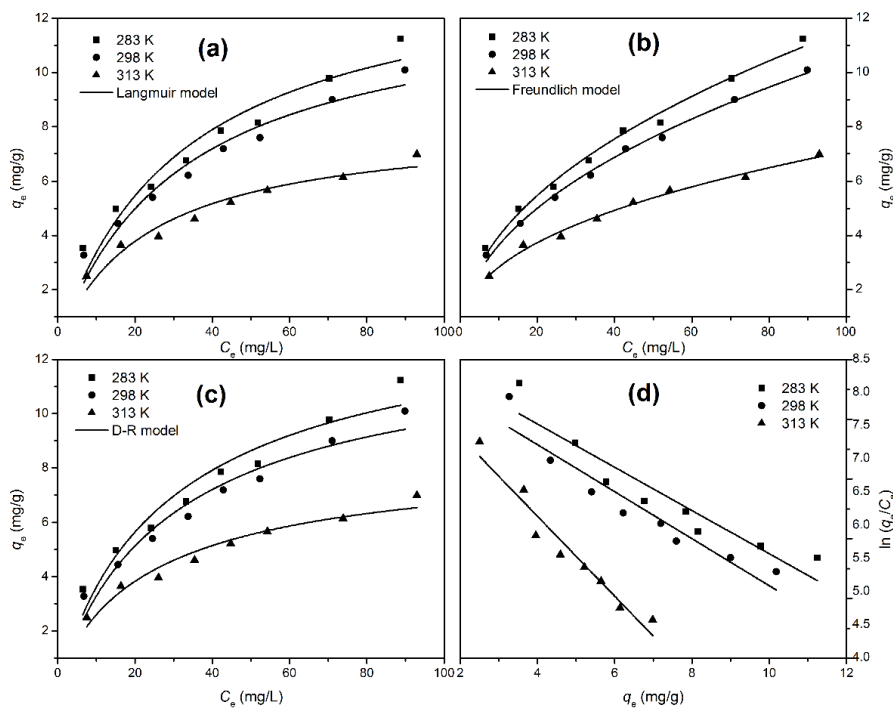


Fig. 8. Nonlinear Langmuir (a), Freundlich (b) and D-R (c) isotherm models at different temperatures for the adsorption of MB onto poorly crystalline HAP nanoparticles; (d) Plots of $\ln q_e/C_e$ vs q_e for the MB adsorption on poorly crystalline HAP at different temperatures (q_e : mg/g, C_e : mg/mL).

The maximum adsorption capacity calculated from D-R model (X_m) were 13.20, 12.04 and 8.03 mg/g at 283, 298 and 313 K, respectively, which were lower than q_m values derived from Langmuir model (Table 1). The X_m derived from D-R model was usually lower than the q_m value of the Langmuir model, which was due to the different definition of the maximum adsorption capacity in the two models [58]. In the Langmuir model, q_m represented the maximum adsorption of MB at monolayer coverage, whereas X_m represented the maximum adsorption of MB at the total specific micropore volume of the adsorbent in D-R model. Energy E was useful for estimating the type of adsorption. It was generally accepted that if the value of E was below 8 kJ/mol the adsorption process was of a physical nature, between 8 and 16 kJ/mol the adsorption type could be explained by ion exchange, and above 16 kJ/mol the adsorption process followed by chemical adsorption [59]. As shown in Table 1, the values of average adsorption energy E lied in the range of 5.09-6.05 kJ/mol for different temperatures. These values were all positive and less than 8.0 kJ/mol, indicating that the removal of MB by poorly crystalline HAP was mainly through physical adsorption.

Table 1. Isotherm constants and correlation coefficients for the adsorption of MB on poorly crystalline HAP at different temperatures

Fitting model	Parameter	Temperature (K)		
		283	298	313
Langmuir	q_m (mg/g)	14.27	12.94	8.17
	K_L (L/mg)	0.0310	0.0313	0.0431
	R^2	0.9239	0.9396	0.9361
Freundlich	K_F (mg/g (L/mg) ^{1/n})	1.36	1.26	1.13
	$1/n$	0.4648	0.4592	0.3994
	R^2	0.9928	0.9950	0.9935
Dubinin-Radushkevich	X_m (mg/g)	13.20	12.04	8.03
	B (mol ² /kJ ²)	0.01913	0.01731	0.01365
	E (kJ/mol)	5.09	5.37	6.05
	R^2	0.9282	0.9435	0.9513

In order to assess the performance of poorly crystalline HAP as an adsorbent for MB, the adsorption capacity and equilibrium time of poorly crystalline HAP were compared with those of other adsorbents examined for the removal of MB in the literature (Table 2). It was found that the adsorption capacity (q_m) of MB on poorly crystalline HAP was higher than many other adsorbents, but it was lower than acid-bound magnetic nanoparticles [24], halloysite nanotubes [28], and ordered mesoporous silica [69], etc. However, MB adsorption by poorly crystalline HAP was very rapid and the adsorption process reached equilibrium only within 2 min, which would facilitate its practical application in economical wastewater treatment. Moreover, the poorly crystalline HAP nanoparticles are low-cost and easy to prepare in large scale, and the environmental risk of HAP itself can be neglected because it has displayed good cytocompatibility [70]. Therefore, poorly crystalline HAP exhibits potential as a new biocompatible adsorbent for the removal of MB from aqueous solution.

Table 2 The comparison of maximum MB adsorption capacities of various adsorbents on the basis of Langmuir isotherm model.

Adsorbent	q_m (mg/g)	Equilibrium time (h)	Adsorbent dosage (g/L)	pH	Temperature (K)	References
HAP	0	0.5	0.2	*	298	20
Fly ash	3.074	1.0	40	7.5	303	60
Posidonia oceanica	5.56	3.0	10	6.0	303	61
Coir pith carbon	5.87	2.0	6.0	6.9	308	62
Clay	6.3	1.0	1.0	*	293	63
Natural phosphate	7.232	1.0	1.0	*	298	64
Neem leaf powder	8.76	5.0	2-10	*	300	65
Activated carbon	9.813	1.0	20	7.5	303	60
Ulva lactuca	10.994	2.0	10	10	298	66
Sawdust	11.8	1.0	4.0	7.0	299	67
Raw kaolin	13.99	3.0	0.8	*	300	68
Poorly crystalline HAP	14.27	2 min	1.0	9.0	283	This study
Ordered mesoporous silica	54.0	12 days	1.0	*	295	69
Halloysite nanotubes	40.82**	72	1.0	*	298	28
Acid-bound magnetic nanoparticles	199	1.0	1.0	*	298	24

* not available, ** obtained from Pseudo-second-order model.

3.6 Thermodynamic analyses

To further evaluate the effect of temperature on the adsorption and investigate the possible mechanism involved in the adsorption process, the thermodynamic behaviors were evaluated by the following equations:

$$\Delta G^0 = -RT \ln K_0 \quad (8)$$

$$\ln K_0 = \frac{\Delta S^0}{R} - \frac{\Delta H^0}{RT} \quad (9)$$

where ΔG^0 is the standard free energy of adsorption (kJ/mol); R is the universal gas constant (8.314 J/(mol·K)); T is the temperature in Kelvin; K_0 is the thermodynamic equilibrium constant; ΔS^0 is the standard entropy change (J/(mol·K)) and ΔH^0 is the standard enthalpy change (kJ/mol). The values of ΔH^0 and ΔS^0 could be obtained from the slope and intercept of a plot of $\ln K_0$ against $1/T$.

Equilibrium constant (K_0) for the adsorption process was determined by plotting $\ln q_e/C_e$ vs q_e and extrapolating to zero q_e using a graphic method described by Khan and Singh [71]. Regression straight lines were fitted through the data points by the least-squares method, and their intersections with the vertical axis gave the value of K_0 (Figure 8d). The calculated values of thermodynamic parameters were shown in Table 3. It was obvious that the ΔG^0 values were all

negative in this study, confirming that the adsorption of MB onto poorly crystalline HAP was spontaneous and thermodynamically favorable. Moreover, it was generally accepted that the change in free energy for physisorption was between -20 and 0 kJ/mol, while chemisorption was a range of -80 to -400 kJ/mol [59]. The obtained values of ΔG^0 were within the range of -20 and 0 kJ/mol, suggesting that the physisorption was likely the main mechanism. Additionally, the negative value for ΔH^0 indicated that the adsorption of MB onto poorly crystalline HAP was an exothermic process, suggesting the MB adsorption process became more favorable at lower temperature. In addition, the positive value of ΔS^0 suggested the increased randomness at the solid-solution interface during the adsorption process of MB onto poorly crystalline HAP. Moreover, the value of ΔS^0 was relatively low, also indicating that the interactions between adsorbent and adsorbate molecules were physical [63].

Table 3. Thermodynamic parameters of the MB adsorption onto poorly crystalline HAP at different temperatures.

Temperature (K)	$\ln K_0$	ΔG^0 kJ/mol	ΔH^0 kJ/mol	ΔS^0 (J/(mol·K))
283	1.8997	-4.470	-0.59	13.70
298	1.8831	-4.666		
313	1.8758	-4.881		

3.7 Regeneration and reuse

In order to evaluate the possibility of regeneration and reuse of the poorly crystalline HAP adsorbent, desorption experiments have been performed. Several desorbing reagents have been reported for desorption of MB from various adsorbents, such as acetic acid [1], HCl [18], KCl [25], and a mixture of methanol and acetic acid [24,26,27]. Since adsorption of MB was very less at low pH as shown in Figure 5a, it could be inferred that acidic solution might aid in desorption of MB from the poorly crystalline HAP nanoparticles. Accordingly, it was generally found that the desorption efficiency of acidic mixture of methanol and acetic acid was greater than that of the other desorption reagents [24,26,27].

However, these acidic agents could not be used for desorption of MB from HAP since solubility of HAP in aqueous media increased with lowering pH value [72]. Alternatively, phosphate buffer including considerably weak acids H_2PO_4^- and HPO_4^{2-} was expected to desorb MB from HAP. It was considered that these phosphate ions had the ability to disturb adsorption of MB molecules on the HAP surface, and to bind strongly to Ca^{2+} of HAP [73]. Therefore, attempts were made to desorb MB from MB-loaded HAP using 0.1 mol/L KH_2PO_4 solution, and desorption efficiencies were compared with different kinds of eluents (distilled water, methanol, KCl). Results indicated the regeneration ability with the KH_2PO_4 solution was found optimum (Figure 9a), and desorption process of MB was achieved within about 5 min, similar to the adsorption equilibrium, which facilitated the fast regeneration of adsorbent. The regenerated HAP samples were reused for four consecutive cycles. Figure 9b showed the recycling of poorly crystalline HAP in the removal of MB. Only a slight loss in adsorption capacity was observed after four cycles of consecutive adsorption-desorption, demonstrating that poorly crystalline HAP was high performance recyclable adsorbent for the removal of MB.

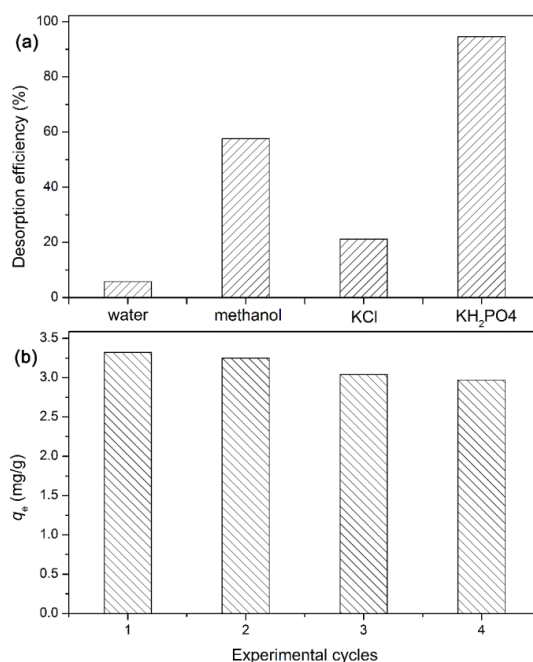


Fig. 9. (a) Desorption efficiencies of MB from poorly crystalline HAP by various desorbing agents; (b) Variation on adsorption capacity in regeneration cycles of poorly crystalline HAP nanoparticles.

4. Conclusions

In this study, the poorly crystalline HAP nanoparticles were prepared by an ultrasound-assisted neutralization method and used as novel adsorbents to remove MB in aqueous solution. Results indicated that MB adsorption by HAP was very rapid and the adsorption process reached a steady state after 2 min. The MB adsorption on the adsorbent was highly dependent on solution pH and temperature, MB adsorption was favored at high solution pH and low temperature. The presence of cations and increased ionic strength had adverse effects on MB sorption. Dissolved organic matter such as HA could significantly promote the adsorption of MB. MB adsorption onto poorly crystalline HAP could be well described by Freundlich model and the maximum adsorption amount of the adsorbent for HA at 283 K was 14.27 mg/g. Thermodynamic calculations showed that the MB adsorption process by poorly crystalline HAP nanoparticles was physisorption, spontaneous and exothermic in nature. Electrostatic interaction, Lewis acid-base interaction, and hydrogen bonding were inferred to be the main mechanisms of MB adsorption by HAP. MB saturated adsorbent could be desorbed in phosphate solution within 5 min and the regenerated adsorbent still possessed high adsorption capacity for MB in solution. The main advantages of poorly crystalline HAP were biocompatible, low-cost, and environmental-friendly nature, and the present findings highlighted that the poorly crystalline HAP nanoparticles could be effectively utilized as promising adsorbents for the removal of MB from aqueous solution.

Acknowledgements

This work is supported by the National Natural Science Foundation of China (Nos. 41303081 and 21307002), the National Programs for High Technology Research and Development of China (No. 2007AA10Z406), the Research Fund for the Doctoral Program of Higher Education (Nos. 20113207110014 and 20133207120019), the Foundation for Talent Recommendation Program of Nanjing Normal University (Nos. 2009103XGQ0063 and 2011105XGQ0247), SRF for ROCS, SEM, and PAPD (a project funded by the Priority Academic Program Development of Jiangsu Higher Education Institutions, No. 164320H116).

References

- [1] M.S. Sajab, C.H. Chia, S. Zakaria, S.M. Jani, M.K. Ayob, K.L. Chee, P.S. Khiew, W.S. Chiu, *Biores. Technol.* **102**, 7237 (2011).
- [2] F. Zhang, Z. Zhao, R. Tan, Y. Guo, L. Cao, L. Chen, J. Li, W. Xu, Y. Yang, W. Song, J. *Colloid Interface Sci.* **386**, 277 (2012).
- [3] J.O. Hao, H. Kim, P.C. Chiang, *Crit. Rev. Environ. Sci. Technol.* **30**, 449 (2000).
- [4] N. Gupta, A.K. Kushwaha, M.C. Chattopadhyaya, *J. Taiwan Inst. Chem. Eng.* **43**, 604(2012).
- [5] M.A., Brown, S.C. de Vito, *Crit. Rev. Environ. Sci. Technol.* **23**, 249 (1993).
- [6] I.K. Kapdan, F. Kargi, *Process Biochem.* **37**, 973 (2002).
- [7] R.K. Prasad, *J. Hazard. Mater.* **165**, 804 (2009).
- [8] E.G. Solozhenko, N.M. Soboleva, V.V. Goncharuk, *Water Res.* **29**, 2206 (1995).
- [9] A. Hu, M. Li, C. Chang, D. Mao, *J. Mol. Catal. A: Chem.* **267**, 79 (2007).
- [10] C.A. Buckley, *Water Sci. Technol.* **25**, 203 (1992).
- [11] M. Panizza, A. Barbucci, R. Ricotti, G. Cerisola, *Sep. Purif. Technol.* **54**, 382 (2007).
- [12] X. Fu, X. Chen, J. Wang, J. Liu, *Microp. Mesop. Mater.* **139**, 8 (2011).
- [13] T.K. Sen, S. Afroze, H.M. Ang, *Water Air Soil Pollut.* **218**, 499 (2011).
- [14] O.M. Paşka, C. Păcurariu, S.G. Muntean, *RSC Adv.* **4**, 62621 (2014).
- [15] L. Cui, Y. Wang, L. Hu, L. Gao, B. Du, Q. Wei, *RSC Adv.* **5**, 9759 (2015).
- [16] T. Akar, B. Anilan, A. Gorgulu, S.T. Akar, *J. Hazard. Mater.* **168**, 1302 (2009).
- [17] G. Ciobanu, S. Ilisei, M. Harja, C. Luca, *Sci. Adv. Mater.* **5**, 1090 (2013).
- [18] S. Saber-Samari, Sa. Saber-Samari, N. Nezafati, K. Yahya, *J. Environ. Manag.* **146**, 481 (2014).
- [19] H. Bouyarmane, S. Saoiabi, A. Laghzizil, A. Saoiabi, A. Rami, M.El. Karbane, *Desal. Water Treat.* **52**: 7265 (2014).
- [20] C. Li, X. Ge, S. Liu, F. Liu, *Adv. Mater. Res.* **463-464**, 543 (2012).
- [21] F. Zhang, W. Song, J. Lan, *Appl. Surface Sci.* **326**, 195 (2015).
- [22] Z.Z. Zhang, M.Y. Li, W. Chen, S.Z. Zhu, N.N. Liu, L.Y. Zhu, *Environ. Pollut.* **158**, 514 (2010).
- [23] Y. Liu, P. Liang, L. Guo, *Talanta* **68**, 25 (2005).
- [24] S.Y. Mak, D.H. Chen, *Dyes Pigments* **61**, 93 (2004).
- [25] R.P. Chen, Y.L. Zhang, X.Y. Wang, C.Y. Zhu, A.J. Ma, W.M. Jiang, *Desal. Water Treat.* doi: 10.1080/19443994.2014.916233, (2014).

- [26] A.Z.M. Badruddoza, G. Si. Hazel, K. Hidajat, M.S. Uddin, *Colloids Surf. A* **367**, 85 (2010).
- [27] X. Zhang, P. Zhang, Z. Wu, L. Zhang, G. Zeng, C. Zhou, *Colloids Surf. A* **435**, 85 (2013).
- [28] M. Zhao, P. Liu, *Microp. Mesop. Mater.* **112**, 419 (2008).
- [29] J. Ma, F. Yu, L. Zhou, L. Jin, M. Yang, J. Luan, Y. Tang, H. Fan, Z. Yuan, J. Chen, *ACS Appl. Mater. Interfaces* **4**, 5749 (2012).
- [30] H.H.A. Ghafar, G.A.M. Ali, O.A. Fouad, S.A. Makhlof, *Desal. Water Treat.* **53**, 2980 (2015).
- [31] L. Ai, C. Zhang, F. Liao, Y. Wang, M. Li, L. Meng, J. Jiang, *J. Hazard. Mater.* **198**, 282 (2011).
- [32] K.G. Scheckel, G.L. Diamond, M.F. Burgess, J.M. Klotzbach, M. Maddaloni, B.W. Miller, C.R., Partridge, S.M. Serda, *J. Toxicol. Environ. Health B Crit. Rev.* **16**, 337 (2013).
- [33] T.S.B. Narasaraju, D.E. Phebe, *J. Mater. Sci.* **31**, 1 (1996).
- [34] R.R. Sheha, *J. Colloid Interface Sci.* **310**, 18 (2007).
- [35] S. Gao, J. Cui, Z.G. Wei, *J. Fluorine Chem.* **130**, 1035 (2009).
- [36] C.S. Sundaram, N. Viswanathan, S. Meenakshi, *J. Hazard. Mater.* **155**, 206 (2008).
- [37] K.L. Lin, J.Y. Pan, Y.W. Chen, R.M. Cheng, X.C. Xu, *J. Hazard. Mater.* **161**, 231 (2009).
- [38] W. Wei, L. Yang, W.H. Zhong, J. Cui, Z.G. Wei, *Appl. Surface Sci.* **332**, 328 (2015).
- [39] T. Bajda, E. Szmit, M. Manecki; L. Pawłowski, M. Dudzińska, A. Pawłowski (Eds.), *Environ. Eng.*, Taylor and Francis, New York, Singapore, 119 (2007).
- [40] N. Barka, S. Qourzal, A. Assabbane, A. Nounah, A.I. Yhya, *J. Environ. Sci.* **20**, 1268 (2008).
- [41] H. El Boujaady, A. El Rhilassi, M. Bennani-Ziatni, R. El Hamri, A. Taitai, J.L. Lacout, *Desalination* **275**, 10 (2011).
- [42] K. Mahmud, Md.A. Islam, A. Mitsionis, T. Albanis, T. Vaimakis, *Desal. Water Treat.* **41**, 170 (2012).
- [43] W. Wei, L. Yang, W. Zhong, J. Cui, Z. Wei, *Digest J. Nanomat. Biostruct.* **10**, 663 (2015).
- [44] S.K. Milonjić, A.Lj. Ruvarac, M.V. Šušić, *Thermochim. Acta* **11**, 261 (1975).
- [45] C. Stötzel, F.A. Müller, F. Reinert, F. Niederdraenk, J.E. Barralet, U. Gbureck, *Colloids Surf. B* **74**, 91 (2009).
- [46] M. Darroudi, H. Eshtiagh-Hosseini, M.R. Housaindokht, *Digest J. Nanomat. Biostruct.* **5**, 29 (2010).
- [47] G.F. Malash, M.I. El-Khaiary, *J. Colloid Interface Sci.* **348**, 537 (2010).
- [48] P. Gramain, J.C. Voegel, M. Gumpfer, J.M. Thomann, *J. Colloid Interface Sci.* **118**, 148 (1987).
- [49] L.M. Wu, W. Forsling, P.W. Schindler, *J. Colloid Interface Sci.* **147**, 178 (1991).
- [50] P. Sharma, M.R. Das, *J. Chem. Eng. Data* **58**, 151 (2013).
- [51] H. Bouyarmane, S.E. Asri, A. Rami, C. Roux, M.A. Mahly, A. Saoiabi, T. Coradinc, A. Laghzizil, *J. Hazard. Mater.* **181**, 736 (2010).
- [52] S. Senthilkumaar, P.R. Varadarajan, K. Porkodi, C.V. Subbhuraam, *J. Colloid Interface Sci.* **284**, 78 (2005).
- [53] R. Han, W. Zou, W. Yu, S. Cheng, Y. Wang, J. Shi, *J. Hazard. Mater.* **141**, 156 (2007).
- [54] Alexro M.M. Vargas, ré L. Cazetta, Marcos H. Kunita, Taís L. Silva, V.C. Almeida, *Chem. Eng. J.* **168**, 722 (2011).
- [55] I. Langmuir, *J. Am. Chem. Soc.* **40**, 1361 (1916).
- [56] H.M.F. Freundlich, *Z. Phys. Chem.* **57**, 385 (1906).
- [57] M.M. Dubinin, L.V. Radushkevich, *Chem. Zentr.* **1**, 875 (1947).

- [58] B. Ma, W.S. Shin, S. Oh, Y.J. Park, S.J. Choi, *Sep. Sci. Technol.* **45**, 453 (2010).
- [59] H. Chen, J. Zhao, G. Dai, *J. Hazard. Mater.* **186**, 1320 (2011).
- [60] V.V. Basava Rao, S.R. Mohan Rao, *Chem. Eng. J.* **116**, 77 (2006).
- [61] M.C. Ncibi, B. Mahjoub, M. Seffen, *J. Hazard. Mater. B* **139**, 280 (2007).
- [62] D. Kavitha, C. Namasivayam, *Bioresour. Technol.* **98**, 14 (2007).
- [63] A. Gürses, S. Karaca, Ç. Doğar, R. Bayrak, M. Açıkyıldız, M. Yalçın, *J. Colloid Interface Sci.* **269**, 310 (2004).
- [64] N. Barka, A. Assabbane, A. Nounah, L. Laanab, Y.A. Ichou, *Desalination* **235**, 264 (2009).
- [65] K.G. Bhattacharyya, A. Sharma, *Dyes Pigments* **65**, 51 (2005).
- [66] A. El Sikaily, A. Khaled, A.E. Nemr, O. Abdelwahab, *Chem. Ecol.* **22**, 149 (2006).
- [67] V.K. Garg, M. Amita, R. Kumar, R. Gupta, *Dyes Pigments* **63**, 243 (2004).
- [68] D. Ghosh, K.G. Bhattacharyya, *Appl. Clay Sci.* **20**, 295 (2002).
- [69] K.Y. Ho, G. McKay, K.L. Yeung, *Langmuir* **19**, 3019 (2003).
- [70] C.C. Ko, M. Oyen, A.M. Fallgatter, J.H. Kim, J. Friction, W.S. Hu, *J. Mater. Res.* **21**, 3090 (2006).
- [71] A.A. Khan, R.P. Singh, *Colloids Surface* **24**, 33 (1987).
- [72] W. Wei, X. Zhang, J. Cui, Z.G. Wei, *Colloids Surf. A* **392**, 67 (2011).
- [73] T. Moriguchi, K. Yano, S. Nakagawa, F. Kaji, *J. Colloid Interface Sci.* **260**, 19 (2003).